# A Computer-Assisted Investigation of a 2-D Array of Chua's Circuits

Fatih Kavaslar and Cüneyt Güzeliş

*Abstract*—**This paper presents simulation results on a 2-D array of coupled Chua's circuits called a chaotic Cellular Neural Network (CNN) in [1], but here will be called an $f(x) - \dot{x}$ coupled chaotic CNN in order to distinguish it from other recently proposed chaotic CNN architectures [2]–[4]. Each isolated cell with unity self-feedback in the network is a Chua's circuit and is connected only to its nearest neighbors defined by a metric and a neighborhood size [1], [5]. The network is designed with a 2-D torus like connection topology having cyclic boundary conditions that play an important role in complete phase syncronization. It is observed in our computer simulations that i) depending on the choice of the intracell parameters and the connection weights, the cells of the network appear to be operating in a double-scroll Chua's attractor, in spiral Chua's attractors, in stable equilibria, in a period-1, a period-2, a large limit-cycle, or in a large chaotic regime, ii) complete phase synchronization in the network with all cells operating in the double scroll regime can be obtained by a suitable choice of the intracell parameters and the feedback connection weights, iii) there is a set of the intracell parameters and connection weights resulting in a chaotic regime such that each cell depending on its constant external input falls into one of the three attractors; namely, the double-scroll, $P^+$ spiral, or $P^-$ spiral Chua's attractor. As a new phenomenon, a close relation between phase synchronization settling-time and input pattern is observed that offers new potentials of Chua's circuit arrays for pattern recognition applications.**

## I. Introduction

NETWORKS OF coupled chaotic subsystems have been investigated as a new paradigm for high-dimensional chaos, for biological neural networks, as well as for information and signal processing [6]–[8]. Among such networks, arrays of Chua's circuits [1]–[4] are gaining particular importance under the motivation of a great deal of investigations on its dynamics and hardware implementations [9]–[12]. In recent studies [2]–[4], synchronization and hyperchaos phenomena have been observed in various arrays of Chua's circuits. This paper reports several qualitatively distinct dynamical regimes and complete phase synchronization phenomena observed in computer simulations of a 2-D array of $f(x) - \dot{x}$ coupled Chua's circuits. This network of coupled Chua's circuits is indeed a 2-D version of the chaotic CNN reported in [1] and constitutes a special case of the generalized CNN's introduced in [5]. It reduces to the CNN [13] upon a modification of some intracell parameters and slopes of the segments in the piecewise-linear output function.

Manuscript received January 15, 1995; revised April 26, 1995. This paper was recommended by Guest Editor L. O. Chua.

The authors are with the Faculty of Electrical-Electronics Engineering, İstanbul Technical University, Maslak 80626, Turkey.

IEEE Log Number 9414468.

The key features of the CNN considered in this paper are: i) the possibility of processing constant and also time-varying 2-D signals fed via external inputs, ii) the possession of a CNN-like connection topology with a space-invariant connection weight pattern, and iii) the possession of an $f(x) - \dot{x}$ type of coupling that ensures the bounded-input bounded-output stability of the whole network, which might have inhibitory connections or excitatory connections.

The 2-D array of $f(x) - \dot{x}$ coupled Chua's circuits considered in this paper differs from other known Chua's circuit arrays [2], [3], [14], [15] in the following respects: i) The models in [2], [3], [14] are 1-D arrays of Chua's circuits; but the chaotic CNN considered in this paper is a 2-D array of Chua's circuits. ii) In the 2-D array of Chua's circuits used in [15], the individual cells are designed not to be operating in the double-scroll regime even when they are isolated. In contrast, each isolated cell in our chaotic CNN operates in the double-scroll regime. iii) As a direct consequence of the unbounded 3-segment piecewise-linear nonlinearity used in the models of [2]–[4], [14], [15], only passive resistive couplings, i.e., only excitatory connections[1] are allowed in these models. The chaotic CNN can have inhibitory connections as well as excitatory connections. iv) The 2-D array model in [4] uses the canonical Chua's circuits as the cells and uses both $z - \dot{x}$ and $x - \dot{z}$ linear couplings. v) The coupling in our chaotic CNN is nonlinear as opposed to other known Chua's circuit arrays [2]–[4], [14], [15]. The output $f(x)$ of each cell in the chaotic CNN is fed to the neighboring cells resulting in a forcing term in the first equation of (1) describing each cell. Therefore, the coupling in the CNN considered in this paper is called an $f(x) - \dot{x}$ coupling.

The state equations describing each cell of the 2-D chaotic CNN considered in this paper is defined by the following dimensionless form:

$$\dot{x}_{i,j} = \alpha \cdot \left[ -\delta \cdot x_{i,j} + y_{i,j} + \sum_{k,l \in \{-1,0,1\}} a_{k,l} \cdot f(x_{i+k,j+l}) + \sum_{k,l \in \{-1,0,1\}} b_{k,l} \cdot u_{i+k,j+l}(t) + I \right] \tag{1}$$

$$\dot{y}_{i,j} = x_{i,j} - y_{i,j} + z_{i,j} \tag{2}$$

$$\dot{z}_{i,j} = -\beta \cdot y_{i,j} \tag{3}$$

[1] The conductance of a passive linear resistor is positive, hence the current passing through this resistor contributes a positive value to the total input of a post-synaptic cell if the output of the associated pre-synaptic cell is positive.

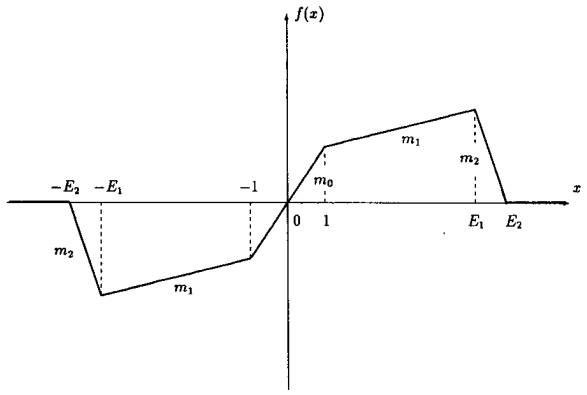


Fig. 1. The characteristics of the 7-segment piecewise-linear function $f(\cdot)$. The outermost zero-slope segments coincide with the horizontal axis.

where

$$f(x) = \frac{1}{2}\cdot(m_0 - m_1)\cdot(|x+1| - |x-1|) + \frac{1}{2}\cdot(m_1 - m_2)\cdot(|x+E_1| - |x-E_1|) + \frac{1}{2}\cdot m_2\cdot(|x+E_2| - |x-E_2|). \quad (4)$$

Here, $i \in \{0,1,2,\ldots,M-1\}$ and $j \in \{0,1,2,\ldots,N-1\}$ for an $M \times N$ network. In order to obtain cyclic boundary conditions, the network is designed as a 2-D torus-like array. As observed from our simulations, cyclic boundary conditions prevent the disturbing effect of boundary conditions on the complete phase synchronization. The external inputs $u_{i,j}(t)$'s might be time-varying. The constant threshold $\mathbf{I}$ is identical for all cells. The $a_{k,l}$ and $b_{k,l}$ coefficients define a space-invariant feedback connection weight pattern and a space-invariant input connection weight pattern, respectively. In the sequel, these coefficients will be specified in the standard matrix forms $A$ and $B$ called the **feedback** and **input** templates, respectively.

$$\mathbf{A} = \begin{bmatrix} a_{-1,-1} & a_{-1,0} & a_{-1,1} \\ a_{0,-1} & a_{0,0} & a_{0,1} \\ a_{1,-1} & a_{1,0} & a_{1,1} \end{bmatrix}$$
$$\mathbf{B} = \begin{bmatrix} b_{-1,-1} & b_{-1,0} & b_{-1,1} \\ b_{0,-1} & b_{0,0} & b_{0,1} \\ b_{1,-1} & b_{1,0} & b_{1,1} \end{bmatrix}. \quad (5)$$

The output function $f(\cdot)$ defined in (4) is a piecewise-linear function different from the original characteristic of the Chua's diode. As can be seen from Fig. 1, the function $f(\cdot)$ is bounded and lies eventually on the $x$-axis. The reason for choosing this bounded function is to ensure the bounded-input bounded-output stability of the overall network for inhibitory connections as well as excitatory connections [1]. On the other hand, such a choice of the output function results in an eventually passive Chua's diode for an isolated cell [1]. The outermost zero-slope segments and the negative-slope segments have no effect on all attractors observed from a three-segment characteristic if $E_1$ is chosen to be less than three. These segments add a large limit-cycle and a large chaotic attractor (see Section II.B) into the dynamical behavior repertoire while ensuring a bounded-input bounded-output stability.

The dimensionless equations in (1)–(4) can be obtained as a two-dimensional special case from the equations defining an $n$-dimensional chaotic CNN [1] by setting the time delays to zero while choosing the neighborhood size equal to one and also making the following changes of variables and parameters: $\tau = \frac{t\cdot G}{C_2}$, $x_{i,j} = \frac{x_{1i,j}}{E_1}$, $y_{i,j} = \frac{x_{2i,j}}{E_1}$, $z_{i,j} = \frac{x_{3i,j}}{E_1\cdot G}$, $\alpha = \frac{C_2}{C_1}$, $\beta = \frac{C_2}{L\cdot G^2}$, $\delta = 1 + \frac{R}{R_N}$, $\bar{m}_o = \frac{m_o}{G}$, $\bar{m}_1 = \frac{m_1}{G}$, $\bar{m}_2 = \frac{m_2}{G}$, $\bar{E}_1 = \frac{E_2}{E_1}$, $\bar{E}_2 = \frac{E_3}{E_1}$. However, the notation $t$, $E_i$'s, and $m_i$'s are used in this paper instead of $\tau$, $\bar{E}_i$'s, and $\bar{E}_i$'s, respectively.

Throughout this paper, the slopes are chosen as $m_0 = \frac{15}{7}$, $m_1 = \frac{12}{7}$, $m_2 = -1$; the breakpoints are located at $E_1 = 20$ and $E_2 = \frac{383}{7}$. For these slopes and breakpoints together with $\delta = 2$ and $a_{o,o} = 1$, an isolated cell of our chaotic CNN when restricted to the region specified by $|x_{i,j}| \le E_1$ becomes identical to the original Chua's circuit. Here, an "isolated" cell is defined as a cell that has no external input and has no connection with other cells. Moreover, in this paper, the term "uncoupled" cell will be used for a cell that has no connection with other cells but has external inputs; and the term "free" cell will be used for a cell that has no external input, and it is not excited by any other cell, but its output is fed to some cells.

All experiments reported in the paper were done for $\mathbf{I} = 0$, $\alpha = 9$, $\delta = 2$. The dynamics of the network are investigated for several choices of connection weights, external inputs, and intracell parameter $\beta$. In all of our simulations, the Forward-Euler method with the step size of 0.001 was used for integrating the differential equations (1)–(4).

Several attractors obtained from an uncoupled cell excited by constant, sinusoidal sources and also by the output of a free cell operating in the double-scroll regime are presented in Section II. An experiment showing a coherent dynamical behavior of all cells operating in the double-scroll regime is also presented in Section II. Simulation results showing a complete phase synchronization and its application to the recognition of lines in images are described in Section III.

## II. Dependence of Dynamics on Connection Weights and Inputs

Our analysis in this section is twofold: one is the analysis of the dynamics of an uncoupled cell as a function of the intracell parameters and inputs; second is the analysis of the overall network based on the connection weights and inputs. The ultimate goal of our analysis is to design a network of identical cells such that the dynamics of a single cell are controlled by an intracell parameter, for instance $\beta$, and the dynamics of the overall network is controlled by the connection weights.

### A. Double-Scroll Chua's Attractor as a Coherent Mode

We first investigate if the double-scroll regime can be a coherent mode of operation for coupled cells each of which is individually designed to be operating in a double-scroll regime. Such a coherent dynamical behavior of all cells in the double-scroll regime was observed in several experiments with different choices of the feedback connection weights and network sizes. One of these experiments was realized for an

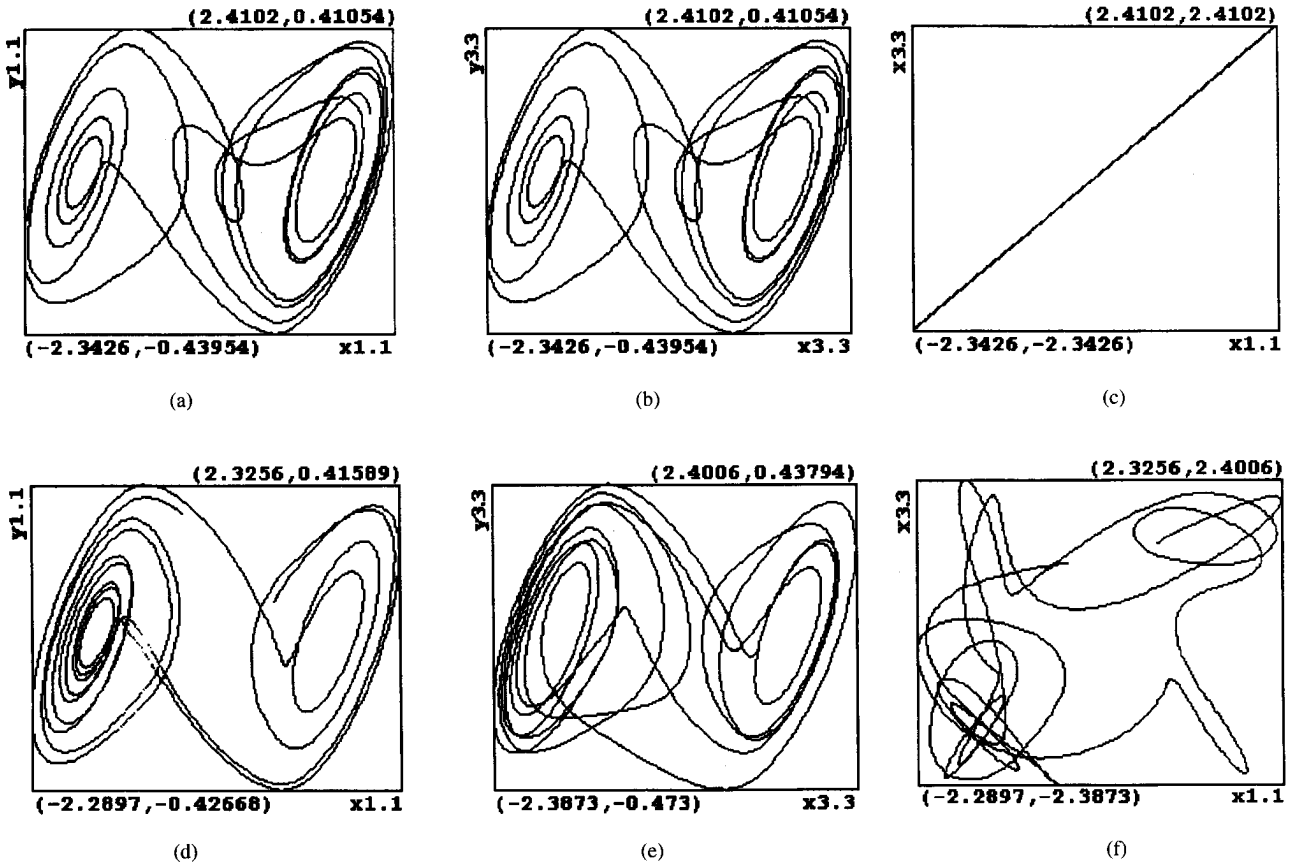


Fig. 2. The trajectory plots (Lissajous figures) for an 8 × 8 chaotic CNN operating in a coherent double-scroll mode. (a) $x$–$y$ trajectory plot for cell $C(1,1)$ under uniform initial conditions. (b) $x$–$y$ trajectory plot for cell $C(3,3)$ under uniform initial conditions. (c) $x$–$x$ trajectory plot for the pair of cells $C(1,1)$ and $C(3,3)$ under uniform initial conditions. (d) $x$–$y$ trajectory plot for cell $C(1,1)$ under nonuniform initial conditions. (e) $x$–$y$ trajectory plot for cell and $C(3,3)$ under nonuniform initial conditions. (f) $x$–$x$ trajectory plot for the pair of cells $C(1,1)$ and $C(3,3)$ under nonuniform initial conditions.

8 × 8 network with $\beta = 14.28$. The templates used are as follows:

$$\mathbf{A}_1 = \begin{bmatrix} 0.001 & 0.001 & 0.001 \\ 0.001 & 1 & 0.001 \\ 0.001 & 0.001 & 0.001 \end{bmatrix}$$
$$\mathbf{B}_1 = \begin{bmatrix} 0 & 0 & 0 \\ 0 & 0 & 0 \\ 0 & 0 & 0 \end{bmatrix}. \quad (6)$$

A set of trajectory plots (Lissajous figures) obtained with the initial conditions $x_{i,j}(0) = y_{i,j}(0) = z_{i,j}(0) = 0.1$ (identical for all cells) is given in Fig. 2(a)–(f). As can be seen from the $x$-$y$ trajectory plots in Fig. 2(a) and (b), the double-scroll regime of the isolated cells with the parameters $\beta = 14.28$ and $a_{o,o} = 1$ is not destroyed in a network of **weakly-coupled** cells. For an identical choice of the initial conditions, not only mode coherence but also the phase coherence was observed. The phase synchronization observed for the pair of cells $C(1,1)$ and $C(3,3)$ is illustrated by the $x$-$x$ trajectory plot in Fig. 2(c). For the above parameters, all cells operate in the same mode and with the same phase. However, for the considered 8 × 8 network, complete phase synchronization is seen to be sensitive to initial conditions so that it may be destroyed by choosing initial conditions which differ from one cell to another. Fig. 2(d)–(f) shows the destruction of the phase coherence between cells $C(1,1)$ and $C(3,3)$ and the preservation of the mode coherency under nonuniform initial conditions. A 3 × 3 network exhibiting complete phase synchronization that is persistent to variations in the initial conditions and external constant inputs will be reported in Section III.

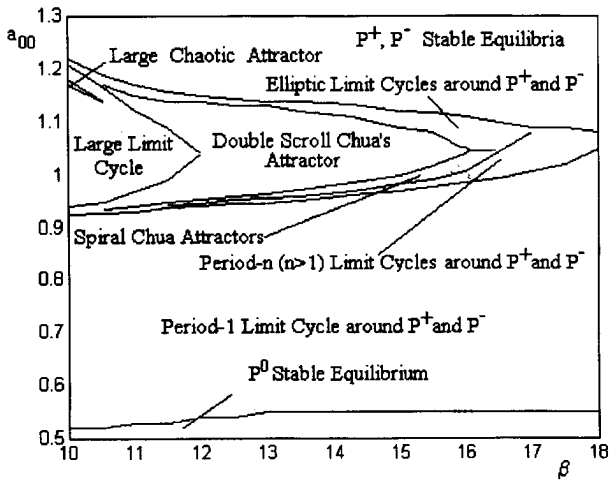


Fig. 3. A rough $\beta - a_{o,o}$ bifurcation diagram.

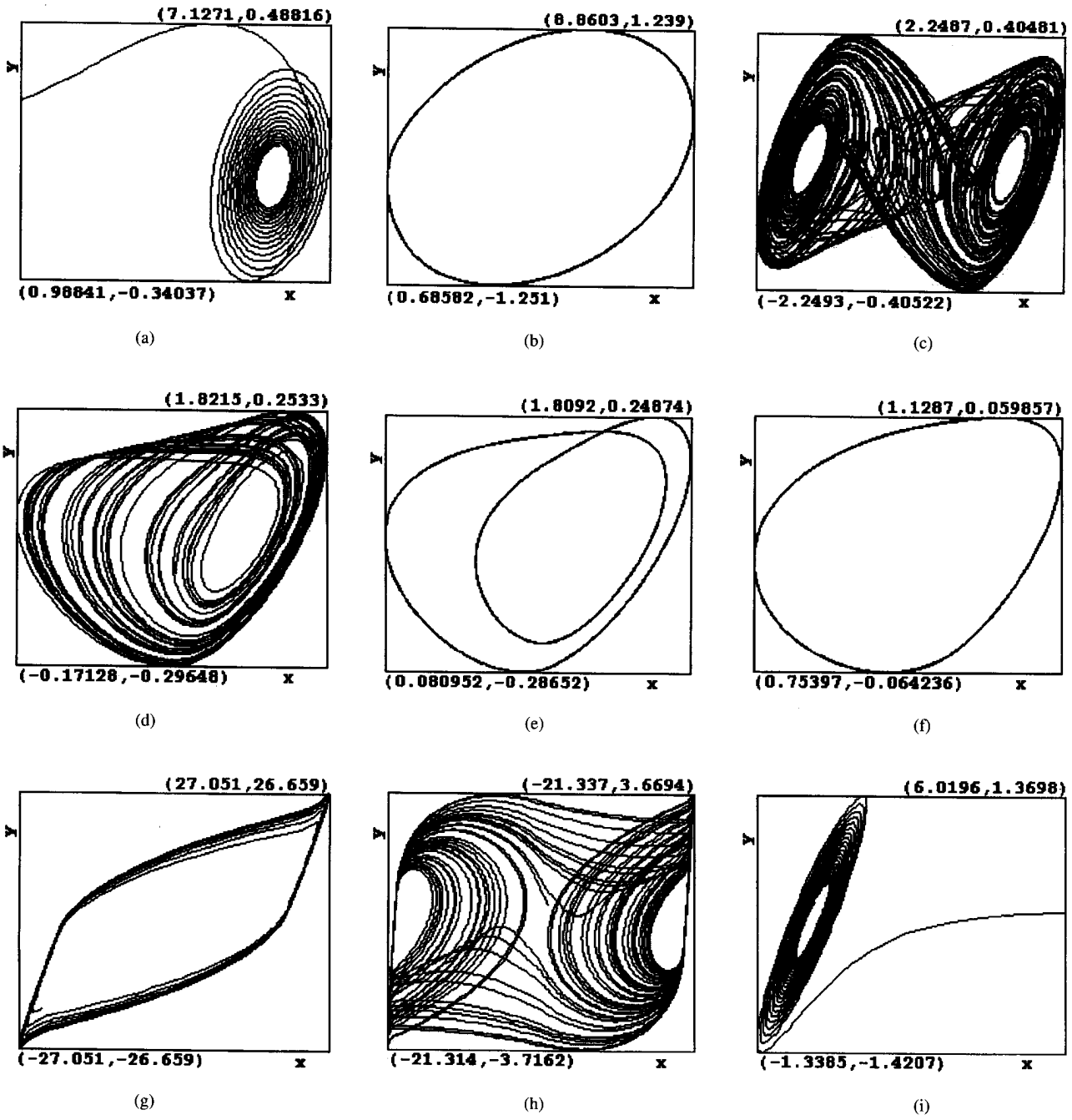


Fig. 4. Typical $x$–$y$ trajectory plots obtained for several choices of $\beta$ and $a_{o,o}$ in an isolated cell. (a) A trajectory converging toward the $P^+$ equilibrium. (b) An elliptic limit-cycle surrounding the $P^+$ equilibrium. (c) A double-scroll Chua's attractor. (d) A $P^+$ spiral Chua's attractor. (e) A period-2 limit-cycle around the $P^-$ equilibrium. (f) A period-1 limit-cycle around the $P^+$ equlibrium. (g) A trajectory converging toward a large limit-cycle. (h) The newly observed large chaotic attractor. (i) A trajectory converging toward the $P^o$ equilibrium.

### *B. Attractors in an Isolated Cell*

Investigation of the coherent modes in the overall network requires the knowledge of the dynamics of an individual cell. An isolated cell with unity self-feedback, i.e., $a_{o,o} = 1$ becomes identical to a Chua's circuit which has been already investigated extensively, thus, there is no need to consider the unity self-feedback case here. However, an isolated cell with $a_{o,o} \neq 1$ differs from the original Chua's circuit and needs to be investigated further.

A set of experiments is done for several choices of the parameters $\beta$ and $a_{o,o}$. The other intracell parameters are as given in Section I, and the templates are

$$\mathbf{A}_2 = \begin{bmatrix} 0 & 0 & 0 \\ 0 & a_{o,o} & 0 \\ 0 & 0 & 0 \end{bmatrix}, \quad \mathbf{B}_2 = \begin{bmatrix} 0 & 0 & 0 \\ 0 & 0 & 0 \\ 0 & 0 & 0 \end{bmatrix}. \tag{7}$$

The bifurcation diagram in Fig. 3 roughly specifies the regions of parameters for which an attractor exists. All attractors

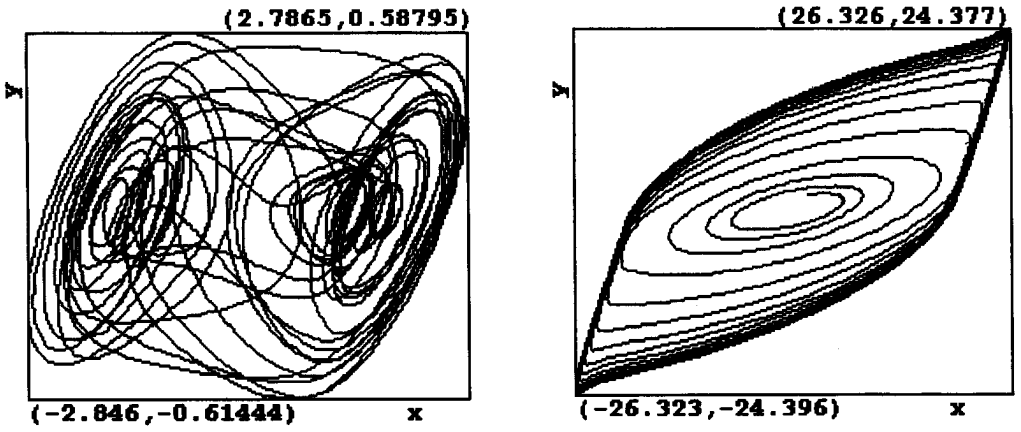


(a) (b)

Fig. 5. The $x$–$y$ trajectory plots for an uncoupled cell driven by a free cell operating in the double-scroll regime. The plots were obtained for 15 000 iteration steps starting from identical initial conditions $x(0) = y(0) = z(0) = 0.1$. (a) The self-input connection weight $b_{o,o}$ is 0.0475. (b) The self-input connection weight $b_{o,o}$ is 0.075.

reported in this diagram have been observed for a set of initial conditions chosen randomly in a bounded set enclosing the origin. The large limit-cycle illustrated in Fig. 4(g) survives for initial conditions chosen outside of this region while all other attractors disappear. Some periodic windows in the double-scroll parameter region were observed but not shown in the diagram. A set of the observed attractors is displayed in Fig. 4. All of the trajectories were obtained for 40 000 iterations starting from the initial conditions $x_{i,j} = y_{i,j} = z_{i,j} = 0.1$ and plotted after discarding some initial transients.

It is interesting to note that the $P^+$, $P^-$, and $P^o$ stable equilibria, the $P^+$ and $P^-$ Chua's spiral attractors, the period-$n$ limit-cycles, the double-scroll Chua's attractor, and the large limit-cycle (see Fig. 4(a)–(g) and (i)) observed in an isolated cell with $a_{o,o} \neq 1$ are also included in the dynamics of the original Chua's circuit. On the other hand, an isolated cell with unity self-feedback possesses all dynamics of the Chua's circuit since they are identical. Furthermore, these dynamics can be produced by an isolated cell not only for unity self-feedback but also for a wide range of self-feedback weights. A new attractor not observed in the original Chua's circuit is the large chaotic attractor shown in Fig. 4(h). This attractor is inherently due to the negative-slope segments.

In the light of our study on the $\beta - a_{o,o}$ bifurcation of the dynamics, one could search for coherent modes in a network of coupled cells all operating in one of the attractors mentioned above. The coherent double-scroll Chua's attractor mode described in Section II.A and the coherent large limit-cycle mode were observed in simulations of several types of couplings. Our investigation of coherent modes was basically *ad hoc*. However, a necessary condition for mode and phase coherency will be given in Section III.

### C. Excitation by Free Cells

The dynamics of an uncoupled cell driven by a free cell operating in a double-scroll regime are of particular interest not only from the point of view of the network dynamics under excitation but also from the coherent double-scroll mode under no excitations. In a coherent double-scroll mode, each cell

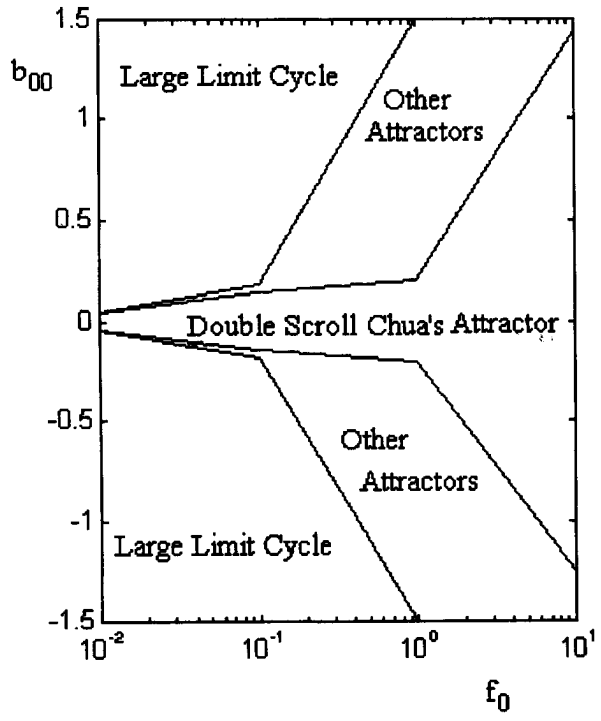


Fig. 6. A rough $f_o - b_{o,o}$ bifurcation diagram.

$C(i,j)$ is excited by a signal $g_{i,j}(t)$ that is a weighted sum of the $f(x_{i,j}(t))$ waveforms associated with the neighboring cells that are all operating in a double-scroll regime. Therefore, an analysis of the cells excited by a free cell provides some insight into the coherent dynamics.

In an experiment done for the following templates and $\beta = 14.28$, it was observed that small input connection weights do not destroy the double-scroll regime as seen in Fig. 5(a). On the other hand, large input connection weights force the cells to be operated in the large limit-cycle as illustrated by Fig. 5(b).

$$\mathbf{A}_3 = \begin{bmatrix} 0 & 0 & 0 \\ 0 & 1 & 0 \\ 0 & 0 & 0 \end{bmatrix}, \quad \mathbf{B}_3 = \begin{bmatrix} 0 & 0 & 0 \\ 0 & b_{o,o} & 0 \\ 0 & 0 & 0 \end{bmatrix}. \tag{8}$$

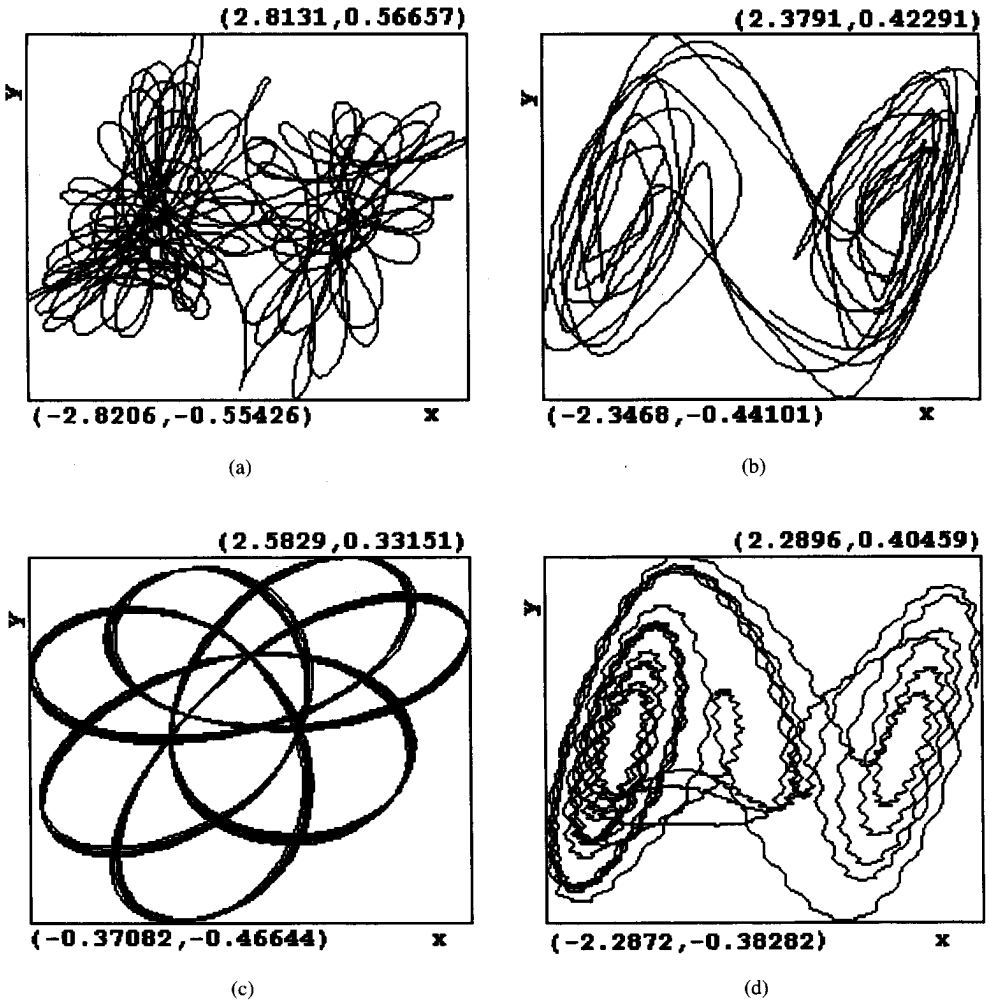


Fig. 7. The $x$–$y$ trajectory plots for an uncoupled cell driven by a sinusoidal oscillator with unit amplitude. The plots were obtained for 40 000 iteration steps starting from identical initial conditions $x(0) = y(0) = z(0) = 0.1$. (a) $f_o = 1$ and $b_{o,o} = 0.6$. (b) $f_o = 1$ and $b_{o,o} = 0.1$. (c) $f_o = 1$ and $b_{o,o} = 0.9$. (d) $f_o = 10$ and $b_{o,o} = 0.3$.

For the above templates, an empirical result for an uncoupled cell to remain in a double-scroll regime when driven by a free cell operating in a double-scroll regime was estimated to be $|b_{o,o}| \leq 0.0475$. On the other hand, the absolute sum of the feedback connection weights excluding the self-feedback being less than 0.0475 can be estimated as a necessary condition for a zero-input network to be in the coherent double scroll mode. Because, in a network of coupled but zero-input cells, the contribution $g_{i,j}(t)$ of the neighboring cells to a cell may be considered as the output of a free cell. Note that the sum 0.008 of the mentioned feedback weights in the experiment of Section II.A is less than 0.0475, which confirms our empirical result.

### D. Excitation by Sinusoidal Oscillators

The dynamics of a single cell under sinusoidal excitations are worth investigating for several reasons. First, monitoring the dynamics helps us to understand the effects of interactions between cells. Second, some unknown coherent periodic modes can be discovered during the process. Third, one may obtain useful information about the use of the whole network for processing periodic signals fed via external inputs.

Several experiments have been performed for the templates in (8) and the attractors observed for several choices of the sinusoidal oscillator frequency $f_o$ and the input template coefficient $b_{o,o}$ are summarized in the $f_o - b_{o,o}$ bifurcation diagram of Fig. 6. Here, $\beta$ has been chosen as 14.28, and the input sinusoidal signal has unity amplitude. Four of the observed attractors are displayed in Fig. 7(a)–(d).

### E. Excitation by Constant Inputs

This part of the experiments is devoted to the analysis of uncoupled cells under constant stimuli. Here, the $\beta$ used is 14.28, and the templates are as follows:

$$\mathbf{A}_4 = \begin{bmatrix} 0 & 0 & 0 \\ 0 & 1 & 0 \\ 0 & 0 & 0 \end{bmatrix}, \quad \mathbf{B}_4 = \begin{bmatrix} 0 & 0 & 0 \\ 0 & 1 & 0 \\ 0 & 0 & 0 \end{bmatrix}. \tag{9}$$

For the above choice of the parameters, a cell under no stimulus is operating in the double-scroll regime as shown in Fig. 8(b). It is also observed that positive (resp. negative) inputs drive the cells into a $P^+$ (resp., $P^-$) spiral Chua's attractor. Such a stimuli-dependent switching from the double-scroll Chua's attractor to the spiral Chua's attractors can be

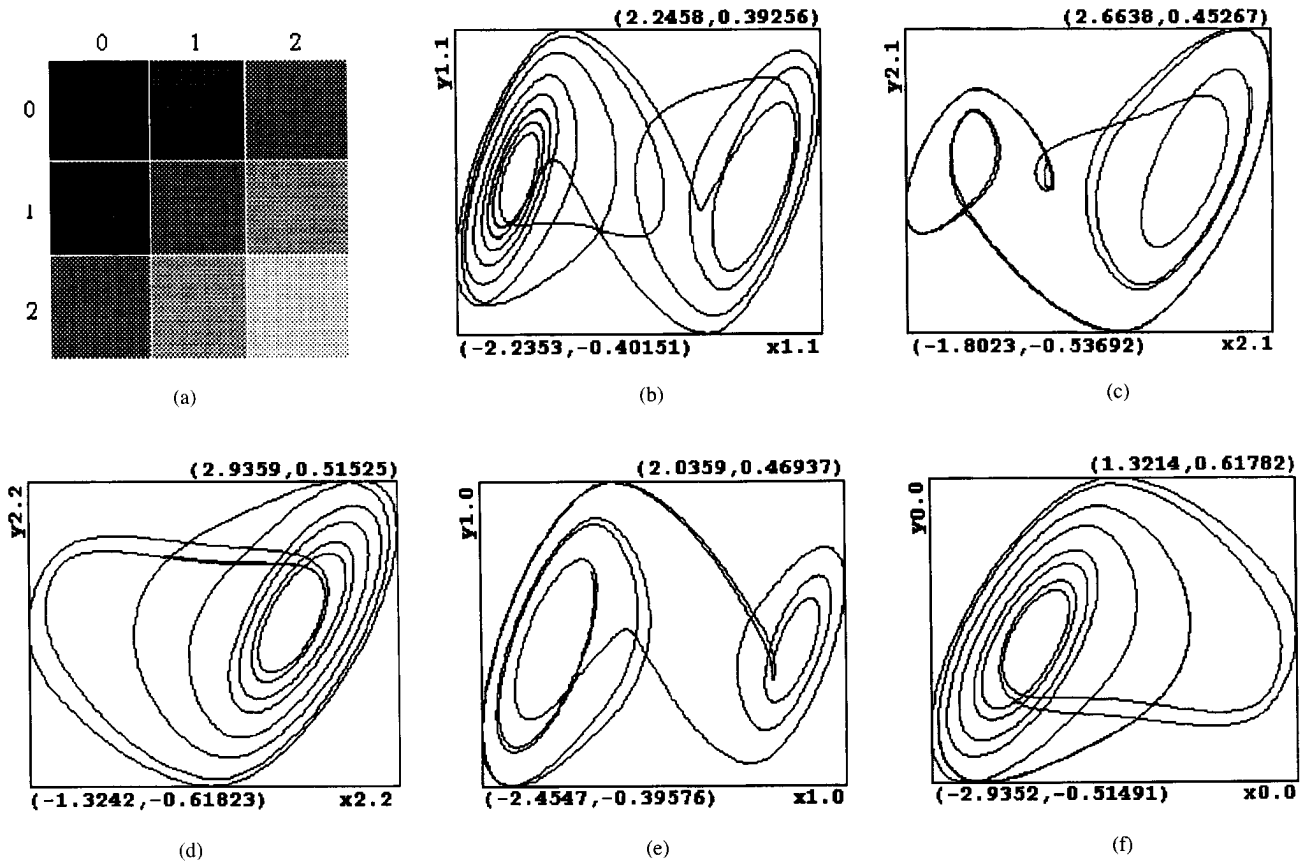


Fig. 8. A 3 × 3 network of uncoupled cells driven by constant inputs. Positive inputs drive the cells into a $P^+$ spiral while negative inputs into a $P^-$ spiral. (a) Image fed to the network as external input. Black corresponds to the input level of −0.125. The other gray levels correspond to−0.025, 0.000, 0.075, and 0.125. (b) The $x$–$y$ trajectory plot for the cell $C(1,1)$. (c) The $x$–$y$ trajectory plot for the cell $C(2,1)$. (d) The $x$–$y$ trajectory plot for the cell $C(2,2)$. (e) The $x$–$y$ trajectory plot for the cell $C(1,0)$. (f) The $x$–$y$ trajectory plot for the cell $C(0,0)$.

useful for classification purposes. Moreover, a network of uncoupled cells can also be used for encoding three-level images such that each level is associated with one of the three chaotic states; namely, double-scroll, $P^+$ and $P^-$ spirals. Fig. 8(a) shows a 3-level gray scale image applied to a 3 × 3 network with the above parameters. The $x$–$y$ trajectory plots for some cells are illustrated in Fig. 8(b)–(f). Note that the upper-left pixel and the mid-left pixel correspond to the cells $C(0,0)$ and $C(0,1)$, respectively; and the other pixels correspond to the remaining cells in the same arrangement.

## III. Phase Synchronization

Phase synchronization has been widely investigated in several arrays of coupled chaotic or periodic oscillators as a phenomenon that may play a role in biological information processing and might be useful for information processing in engineering applications. Complete, partial, and turbulent phase synchronizations have been observed in some arrays and coding of distinct objects as clusters of synchronized subsystems has been proposed as a possible application.

In our experiments, phase synchronizations were observed in the coherent double-scroll mode and in the coherent large limit-cycle mode. We present below simulation results only for a 3 × 3 network exhibiting a persistent complete phase synchronization in the coherent double scroll mode. The $\beta$ used is 14.28, and the templates are as follows:

$$\mathbf{A}_5 = \begin{bmatrix} 0.04 & 0.04 & 0.04 \\ 0.04 & 0.68 & 0.04 \\ 0.04 & 0.04 & 0.04 \end{bmatrix}, \quad \mathbf{B}_5 = \begin{bmatrix} 0 & 0 & 0 \\ 0 & 0 & 0 \\ 0 & 0 & 0 \end{bmatrix}. \tag{10}$$

The 2-level 3 × 3 image in Fig. 9(a) was applied to the network as a set of initial conditions common for all $x$, $y$, and $z$ states variables, i.e., $x_{i,j}(0) = y_{i,j}(0) = z_{i,j}(0)$ for all $i$, $j$. Four different snap shots showing the evolution of the $x$–$x$ trajectory plot belonging to the cells $C(0,0)$ and $C(1,1)$ are illustrated in Fig. 9(b)–(e). As also observed in many other simulations, nonuniform choices of the initial conditions across the network do not annihilate the complete phase synchronization but cause some transition periods before synchronization is achieved. The complete phase synchronization observed is also persistent to variations of the initial conditions from one state variable to another in the same cell.

### A. A Necessary Condition for Phase Coherency

The complete phase synchronization in the double-scroll mode reported above has also been observed for many 3 × 3 networks with the same parameters and the feedback

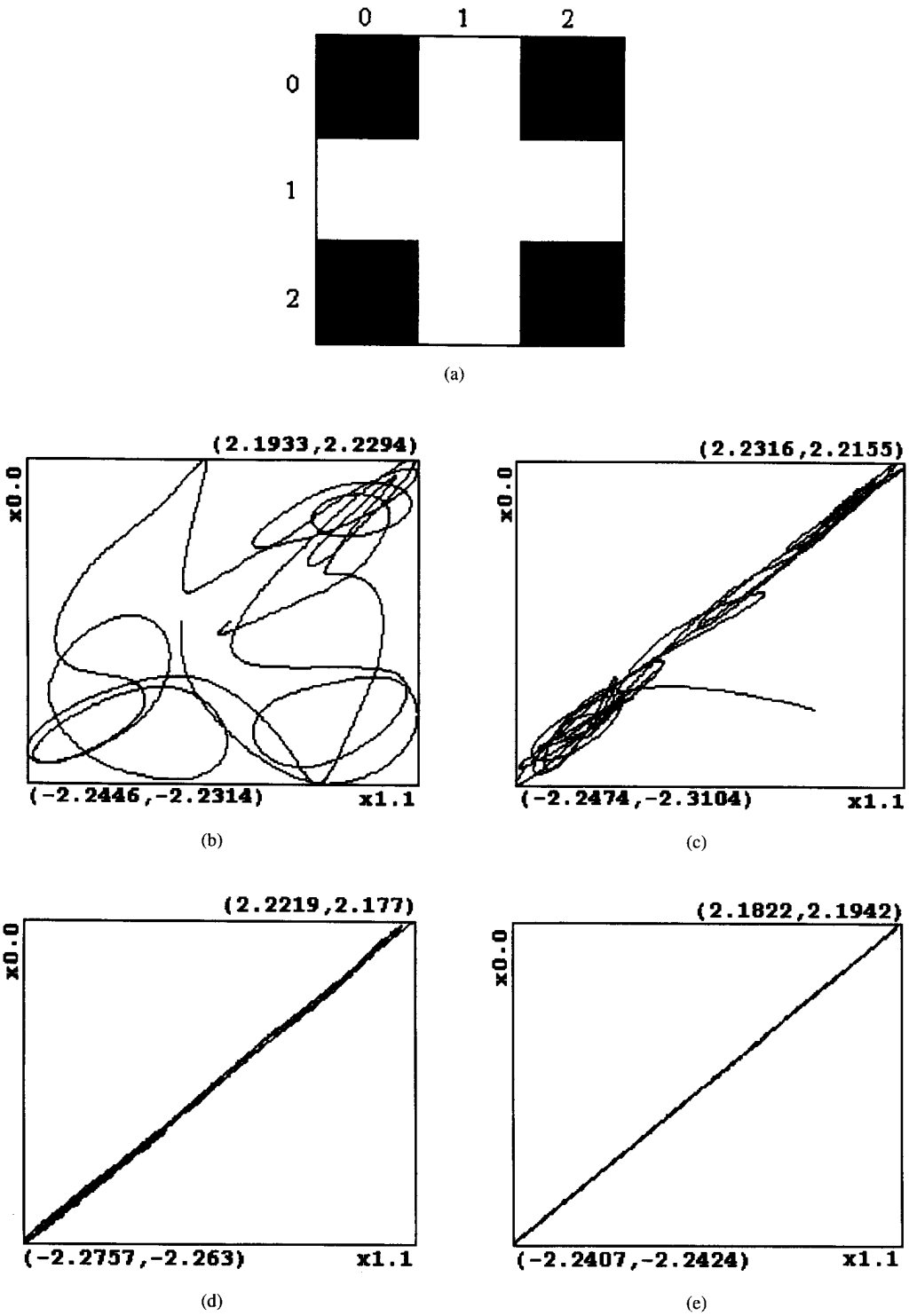


Fig. 9. Complete phase synchronization obtained by the $\mathbf{A}_5 - \mathbf{B}_5$ templates. (a) The 3 × 3 image represents the initial conditions. Black and white correspond to the zero and 0.1 levels, respectively. (b) First snap shot showing the $x_{1,1}-x_{0,0}$ trajectory plot for the period that covers 30 000 iterations before the cells are coupled. (c) Second snap shot showing the $x_{1,1}-x_{0,0}$ trajectory plot for the period that covers 30 000 iterations after the cells are coupled. (d) Third snap shot showing the $x_{1,1}-x_{0,0}$ trajectory plot for the period that covers 30 000 iterations beginning at 30 000th iteration after the cells are coupled. (e) Fourth snap shot showing the $x_{1,1}-x_{0,0}$ trajectory plot for the period that covers 30 000 iterations beginning at 60 000th iteration after the cells are coupled.

connection weights satisfying the condition $W = 1$. Here, $W$ is defined as

$$W = \sum_{k,l\in\{-1,0,1\}} a_{k,l}. \tag{11}$$

Indeed, phase coherency in the double-scroll mode has appeared for $W$'s chosen from the set $D$. Here, $D$ denotes the set of $a_{o,o}$ values such that an isolated cell with a self-feedback weight chosen from $D$ operates in the double-scroll regime. It can be shown by simple analysis that the condition of $W \in D$

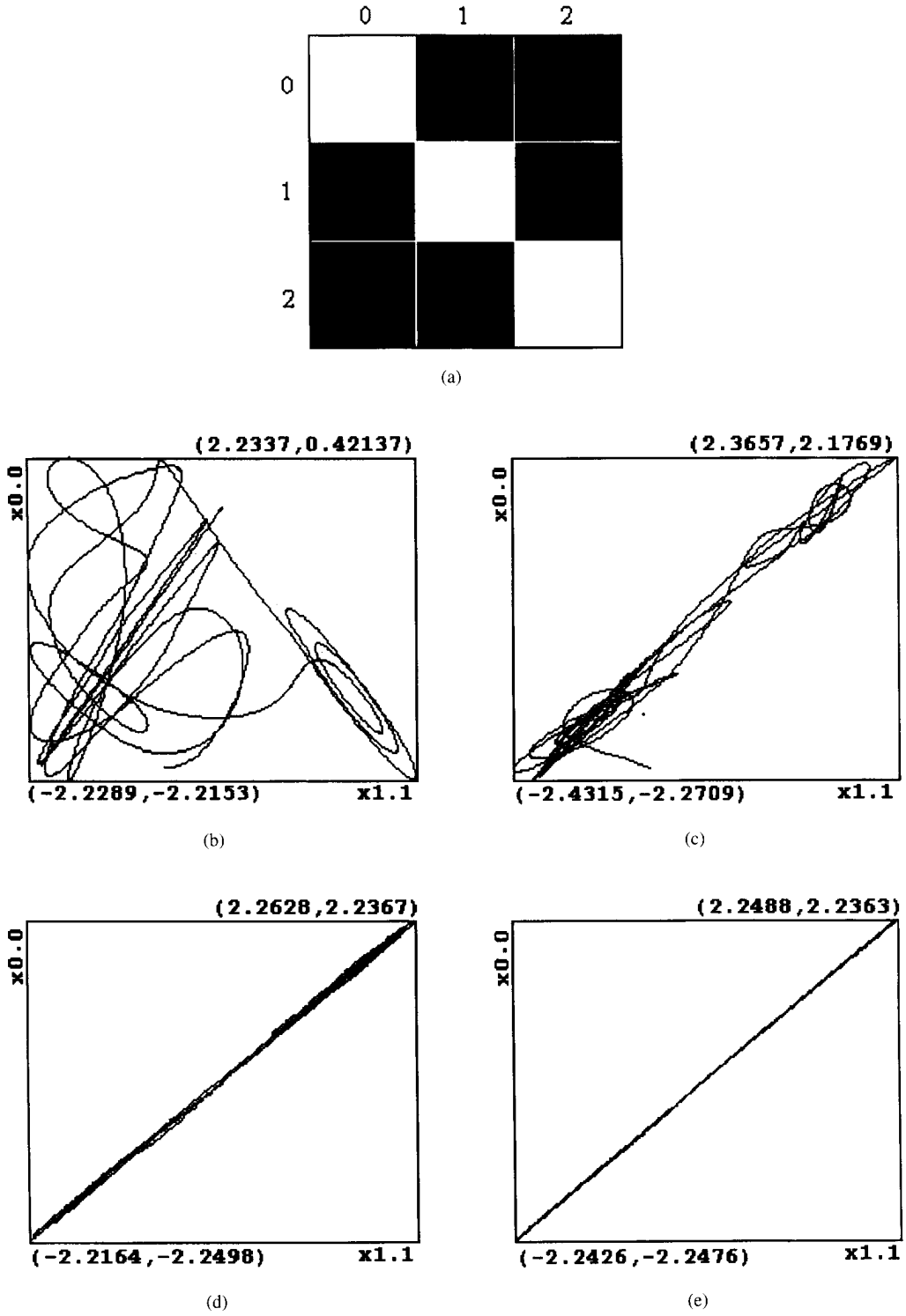


Fig. 10. Fast synchronization depending on the external inputs. The templates are $\mathbf{A}_6 - \mathbf{B}_6$. (a) 3 × 3 image containing a diagonal line with slope $m = -1$ represents the external inputs. Black and white correspond to the zero and 0.1 levels, respectively. (b) A snap shot showing the $x_{1,1}$–$x_{0,0}$ trajectory plot for the period that covers 30 000 iterations before the cells are coupled. (c) A snap shot showing the $x_{1,1}$–$x_{0,0}$ trajectory plot for the period that covers 30 000 iterations after the cells are coupled. (d) A snap shot showing the $x_{1,1}$–$x_{0,0}$ trajectory plot for the period that covers 30 000 iterations beginning at 30 000th iteration after the cells are coupled. (e) A snap shot showing the $x_{1,1}$–$x_{0,0}$ trajectory plot for the period that covers 30 000 iterations beginning at 60 000th iteration after the cells are coupled.

is, indeed, a necessary condition for a network with zero-input to be phase coherent in the coherent double-scroll mode. To do so, let us assume that $x_{i,j}(t) = x(t)$, $y_{i,j}(t) = y(t)$, and $z_{i,j}(t) = z(t)$ for all $t$ as required for complete phase synchronization under uniform initial conditions. Now, the dynamics of the overall network are described by the following

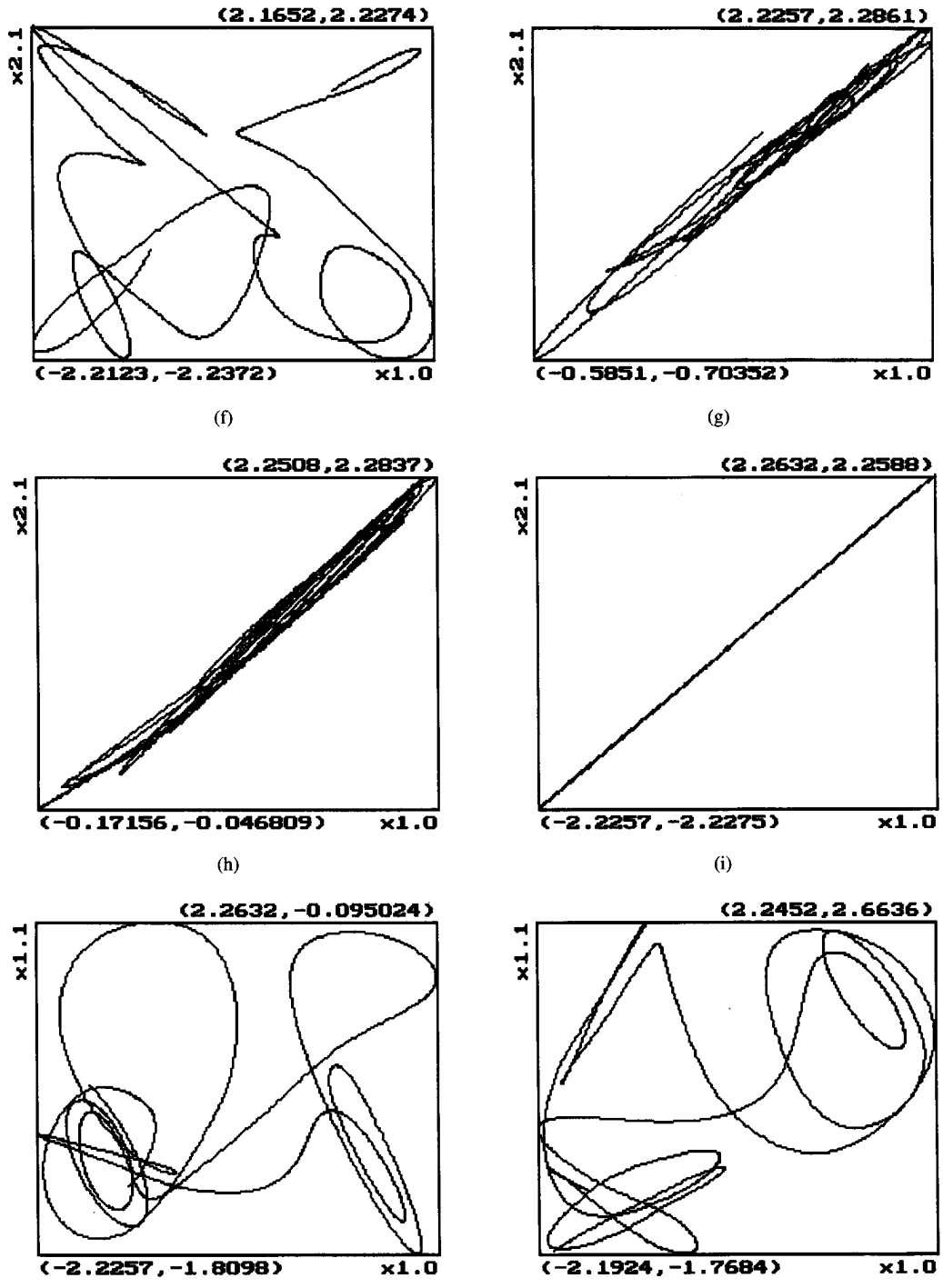


Fig. 10. *(Continued.)* (f) A snap shot showing the $x_{1,0}$–$x_{2,1}$ trajectory plot for the period that covers 30 000 iterations before the cells are coupled. (g) A snap shot showing the $x_{1,0}$–$x_{2,1}$ trajectory plot for the period that covers 30 000 iterations after the cells are coupled. (h) A snap shot showing the $x_{1,0}$–$x_{2,1}$ trajectory plot for the period that covers 30 000 iterations beginning at 30 000th iteration after the cells are coupled. (i) A snap shot showing the $x_{1,0}$–$x_{2,1}$ trajectory plot for the period that covers 30 000 iterations beginning at 60 000th iteration after the cells are coupled. (j) A snap shot showing the $x_{1,0}$–$x_{1,1}$ trajectory plot for the period that covers 30 000 iterations before the cells are coupled. (k) A snap shot showing the $x_{1,0}$–$x_{1,1}$ trajectory plot for the period that covers 30 000 iterations beginning at 60 000th iteration after the cells are coupled.

three differential equations only:

$$\dot{x} = \alpha \cdot \left[ -\delta \cdot x + y + \left( \sum_{k,l \in \{-1,0,1\}} a_{k,l} \right) \cdot f(x) \right] \quad (12)$$

$$\dot{y} = x - y + z \quad (13)$$

$$\dot{z} = -\beta \cdot y. \quad (14)$$

As can easily be seen, the equations in (12)–(14) define an isolated cell. Here, $W$ specifies the self-feedback connection weight $a_{o,o}$ of an isolated cell, hence the condition of $W \in D$ yields the double-scroll regime. This proves the necessity.

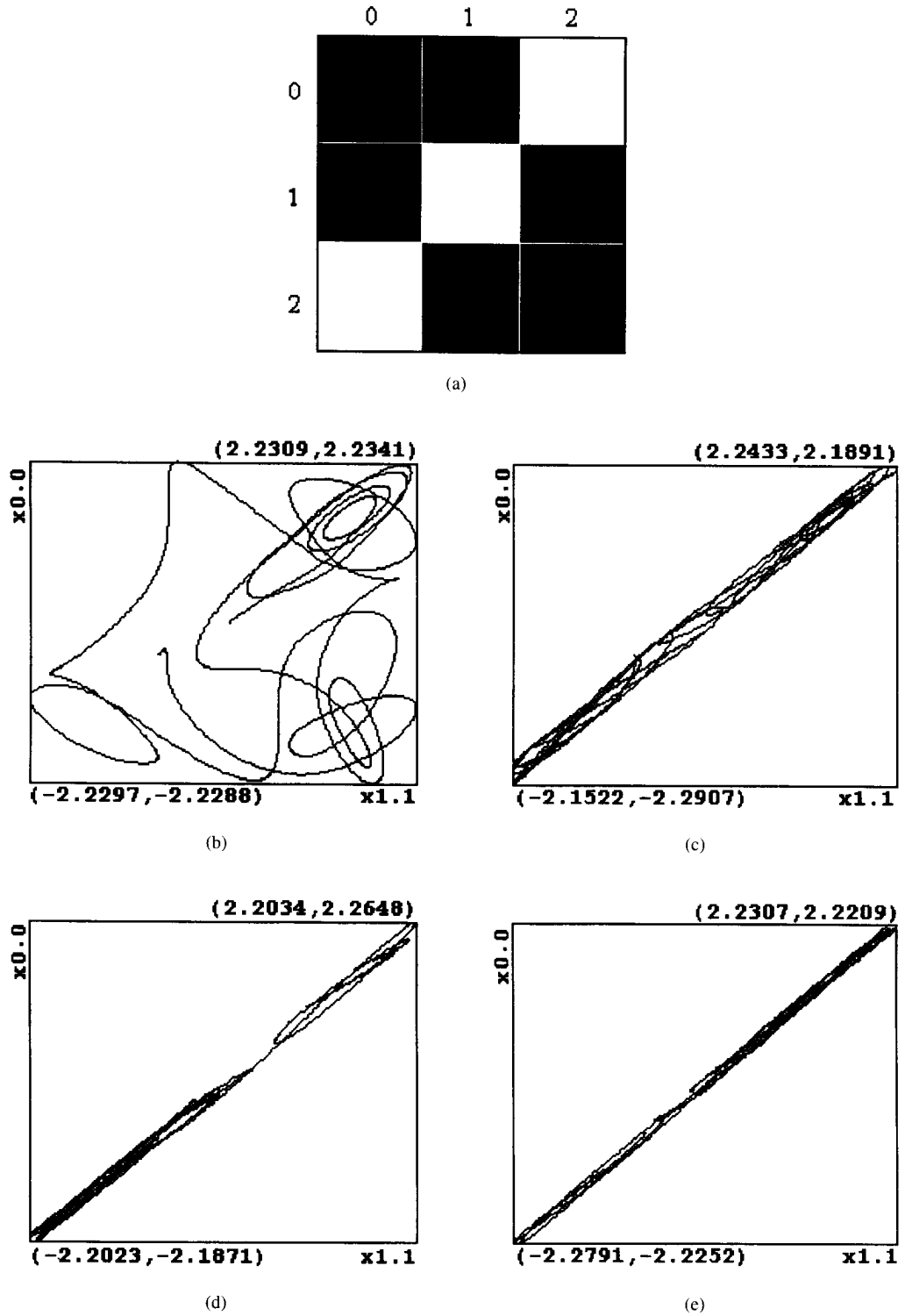


Fig. 11. Slow synchronization depending on the external inputs. The templates are $\mathbf{A}_6 - \mathbf{B}_6$. (a) 3 × 3 image containing a line with slope $m = +1$ represents the external inputs. Black and white correspond to the zero and 0.1 levels, respectively. (b) First snap shot showing the $x_{1,1}$–$x_{0,0}$ trajectory plot for the period that covers 30 000 iterations before the cells are coupled. (c) Second snap shot showing the $x_{1,1}$–$x_{0,0}$ trajectory plot for the period that covers 30 000 iterations after the cells are coupled. (d) Third snap shot showing the $x_{1,1}$–$x_{0,0}$ trajectory plot for the period that covers 30 000 iterations beginning at 30 000th iteration after the cells are coupled. (e) Fourth snap shot showing the $x_{1,1}$–$x_{0,0}$ trajectory plot for the period that covers 30 000 iterations beginning at 60 000th iteration after the cells are coupled.

Similar conditions on $W$ for other coherent modes can be obtained in a same way by considering the $\beta - a_{o,o}$ bifurcation diagram.

### *B. Recognition of Lines via Phase Synchronization*

In the simulations done for the above 3 × 3 network, it was also observed that i) the complete and partial phase

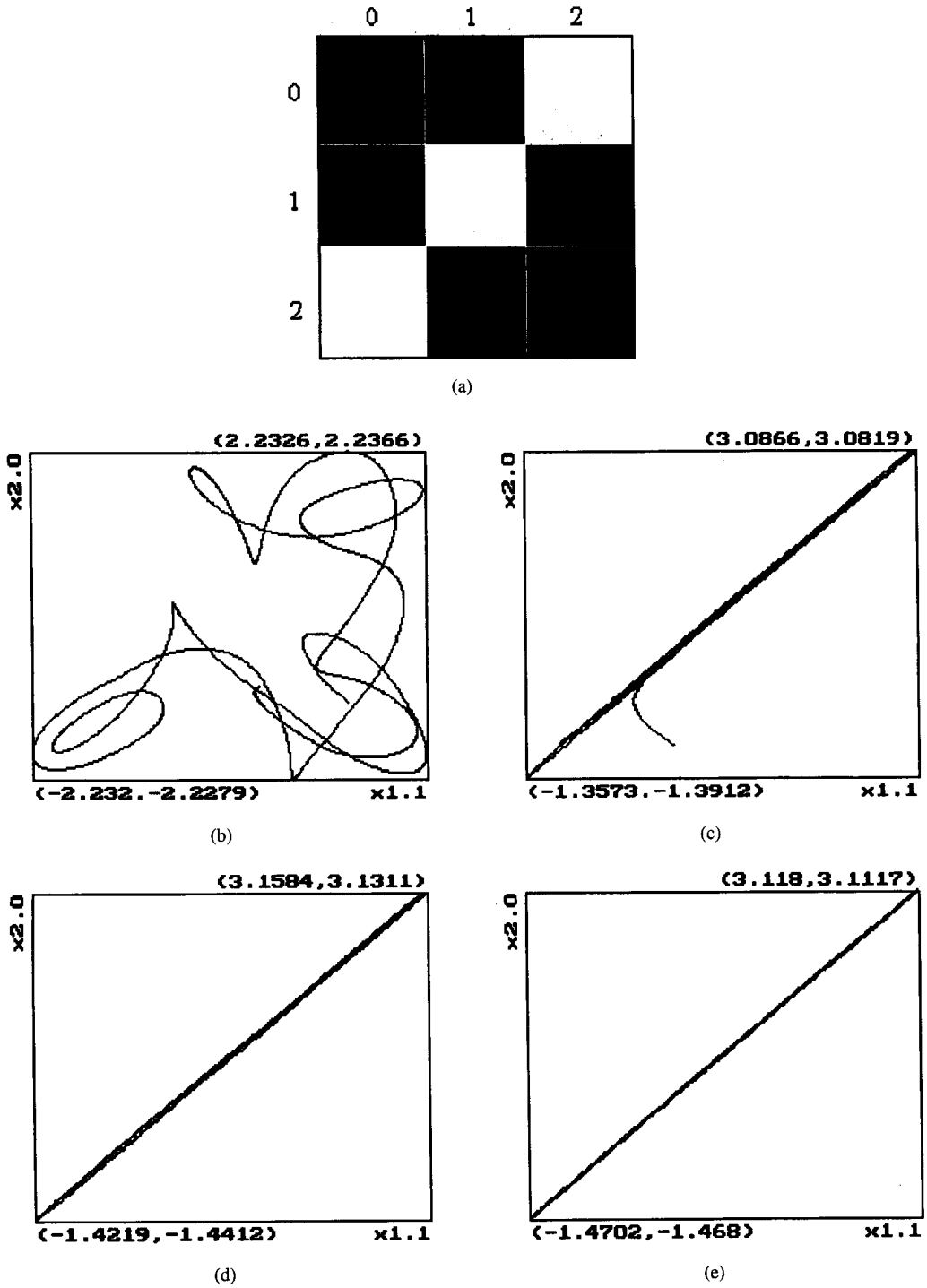


Fig. 12. Fast synchronization depending on the external inputs. The templates are $\mathbf{A}_7 - \mathbf{B}_7$. (a) $3 \times 3$ image containing a line with slope $m = +1$ represents the external inputs. Black and white correspond to the zero and 0.1 levels, respectively. (b) First snap shot showing the $x_{1,1}$–$x_{2,0}$ trajectory plot for the period that covers 30 000 iterations before the cells are coupled. (c) Second snap shot showing the $x_{1,1}$–$x_{2,0}$ trajectory plot for the period that covers 30 000 iterations after the cells are coupled. (d) Third snap shot showing the $x_{1,1}$–$x_{2,0}$ trajectory plot for the period that covers 30 000 iterations beginning at 30 000th iteration after the cells are coupled. (e) Fourth snap shot showing the $x_{1,1}$–$x_{2,0}$ trajectory plot for the period that covers 30 000 iterations beginning at 60 000th iteration after the cells are coupled.

syncronizations in the coherent double scroll mode can survive even under time-invariant inputs, ii) phase synchronization settling-time depends on the inputs presented, and iii) in a partial synchronization regime, the organization of clusters of synchronized cells can be determined by suitable choices of the feedback templates.

The relations between the organization of phase clusters and the type of feedback templates, and between phase synchronization settling-time and patterns fed via external inputs, provide new potentials for pattern recognition. A simple line detection application of the above observed phenomena is presented below.

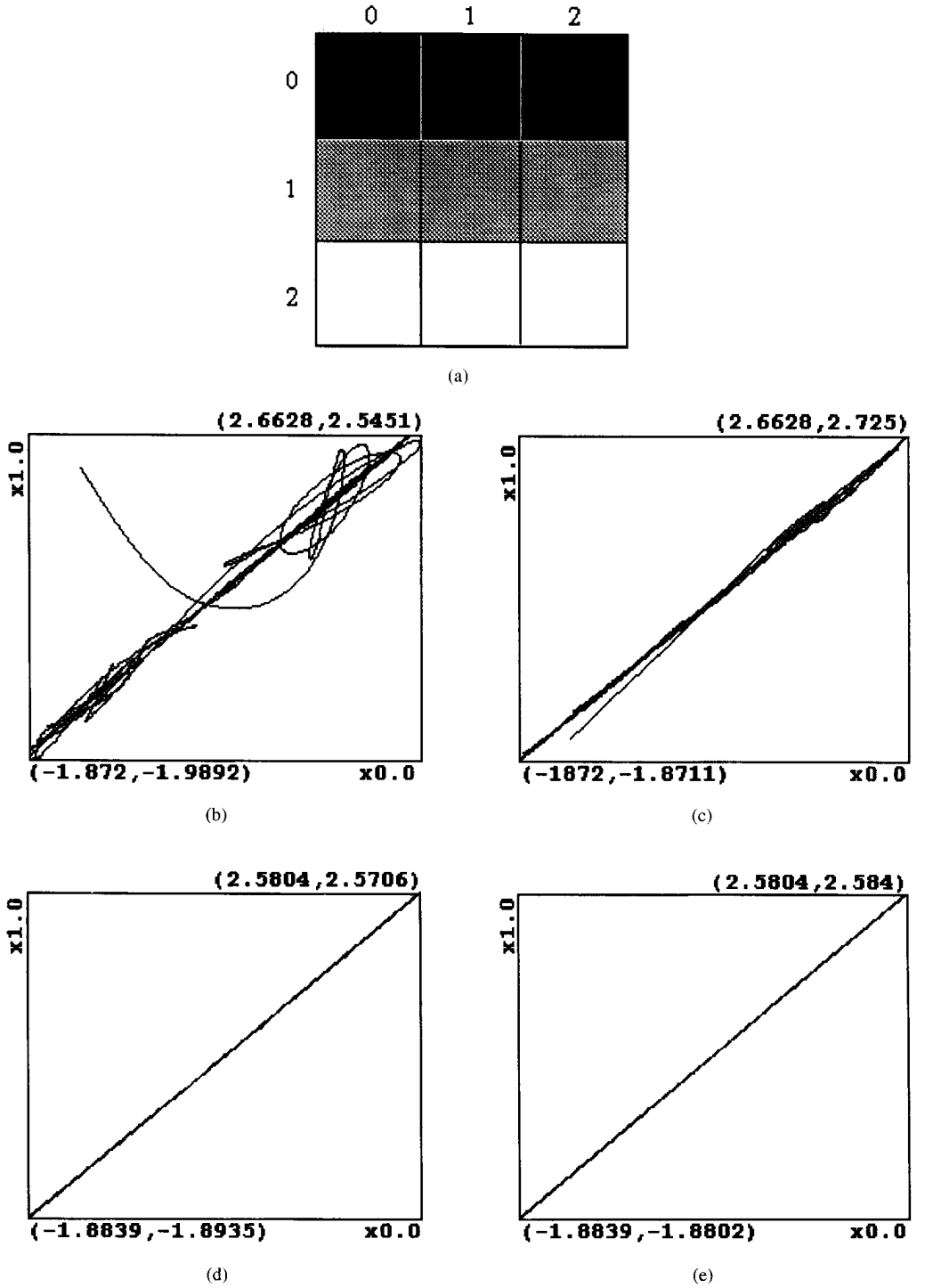


Fig. 13. Fast synchronization of the horizontal neighboring cells for the templates $\mathbf{A}_8 - \mathbf{B}_8$. (a) 3 × 3 image composed of horizontal lines represents the external inputs. Black, white, and the third gray tone correspond to the zero, 0.10, and 0.05 levels, respectively. (b) A snap shot showing the $x_{0,0}$–$x_{1,0}$ trajectory plot for the period that covers 30 000 iterations after the cells are coupled. (c) A snap shot showing the $x_{0,0}$–$x_{1,0}$ trajectory plot for the period that covers 30 000 iterations beginning at 30 000th iteration after the cells are coupled. (d) A snap shot showing the $x_{0,0}$–$x_{1,0}$ trajectory plot for the period that covers 30 000 iterations beginning at 60 000th iteration after the cells are coupled. (e) A snap shot showing the $x_{0,0}$–$x_{1,0}$ trajectory plot for the period that covers 30 000 iterations beginning at 90 000th iteration after the cells are coupled.

In our experiment, the image in Fig. 10(a) is fed via the external inputs to a 3 × 3 network having the templates

$$\mathbf{A}_6 = \begin{bmatrix} 0.13 & 0 & 0 \\ 0 & 0.74 & 0 \\ 0 & 0 & 0.13 \end{bmatrix}, \quad \mathbf{B}_6 = \begin{bmatrix} 0 & 0 & 0 \\ 0 & 0.05 & 0 \\ 0 & 0 & 0 \end{bmatrix}. \quad (15)$$

Different snap shots showing the evolution of an $x$–$x$ trajectory plot associated with two cells along the diagonal (with slope $m = -1$) are given in Fig. 10(b)–(e). Each snap shot covers a period of time requiring 30 000 iterations. The first snap shot shows the period before the cells are coupled.

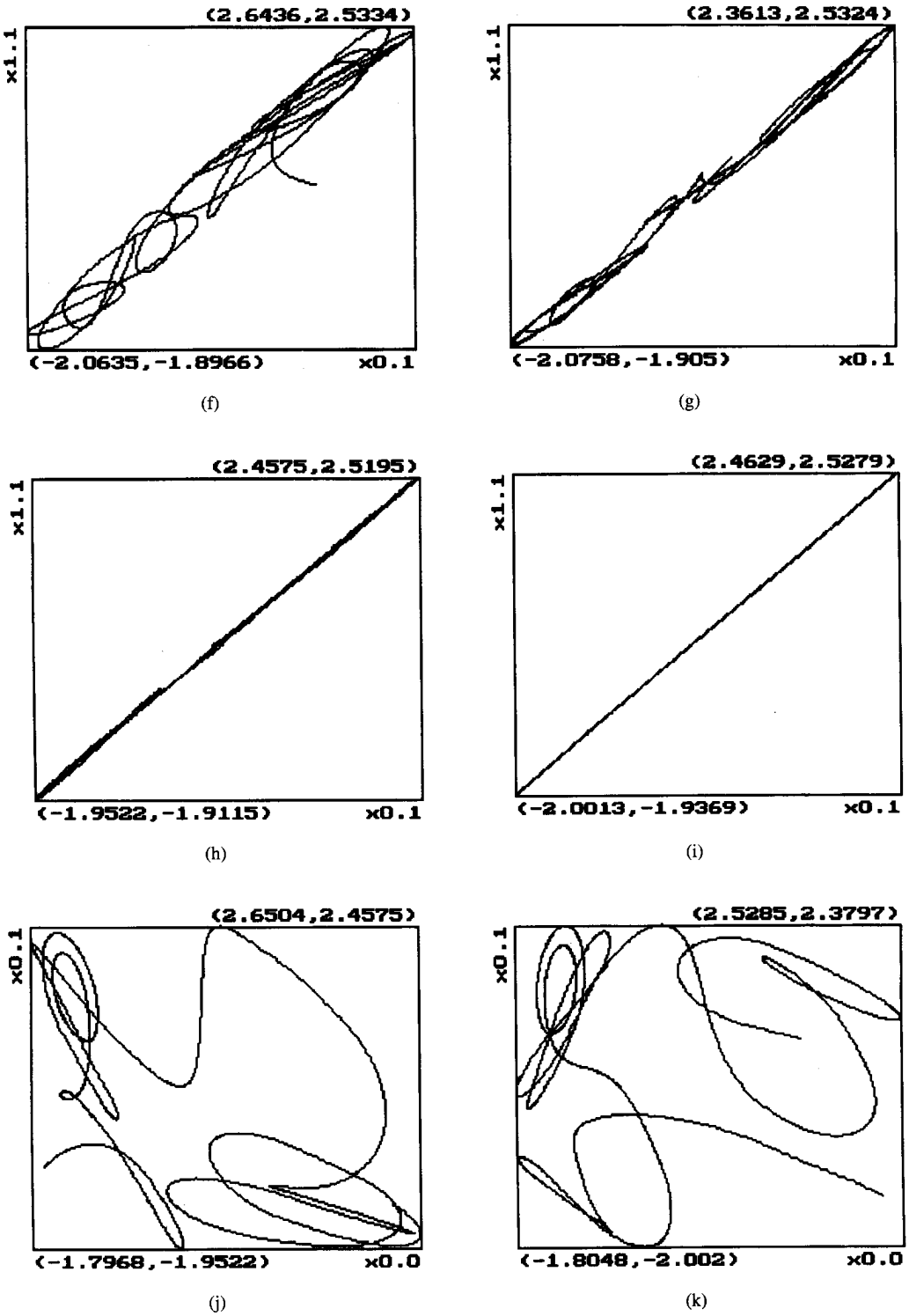


Fig. 13. *(Continued.)* (f) A snap shot showing the $x_{0,1}$–$x_{1,1}$ trajectory plot for the period that covers 30 000 iterations after the cells are coupled. (g) A snap shot showing the $x_{0,1}$–$x_{1,1}$ trajectory plot for the period that covers 30 000 iterations beginning at 30 000 after the cells are coupled. (h) A snap shot showing the $x_{0,1}$–$x_{1,1}$ trajectory plot for the period that covers 30 000 iterations beginning at 60 000th iteration after the cells are coupled. (i) A snap shot showing the $x_{0,1}$–$x_{1,1}$ trajectory plot for the period that covers 30 000 iterations beginning at 90 000th iteration after the cells are coupled. (j) A snap shot showing the $x_{0,0}$–$x_{0,1}$ trajectory plot for the period that covers 30 000 iterations after the cells are coupled. (k) A snap shot showing the $x_{0,0}$–$x_{0,1}$ trajectory plot for the period that covers 30 000 iterations beginning at 60 000th iteration after the cells are coupled.

After that instant, 60 000 iterations were sufficient for the cells $C(0,0)$ and $C(1,1)$ to become synchronized. As shown in Fig. 10(f)–(i), not only cells along the diagonal (with slope $m = -1$) but also cells along any line with slope $m = -1$ become synchronized after 60 000 iterations. Any pair of cells that are not lower-right or upper-left neighbors of each other have never been observed to synchronize (see Fig. 10(j) and (k)). The reason is that such cells are uncoupled for the

template $\mathbf{A}_6$. The same experiment was repeated for the image in Fig. 11(a). As can be seen from Fig. 11(b)–(e), 90 000 iterations (30 000 per snap shot) were not sufficient even for the cells along the diagonal (with slope $m = -1$) to become synchronized. The results obtained in other experiments done for different input images show that the phase synchronization settling-time becomes minimum for the lines with slope $m = -1$. Such a fast stimuli-dependent synchronization indicates the existence of a line (with slope $m = -1$) over the pixels corresponding to the synchronized cells.

This application has been extended to recognize other patterns in the images. It was observed that the following $\mathbf{A}_7 - \mathbf{B}_7$ and $\mathbf{A}_8 - \mathbf{B}_8$ templates can be used for recognizing lines with slope $m = +1$ and horizontal lines, respectively:

$$\mathbf{A}_7 = \begin{bmatrix} 0 & 0 & 0.13 \\ 0 & 0.74 & 0 \\ 0.13 & 0 & 0 \end{bmatrix}, \quad \mathbf{B}_7 = \begin{bmatrix} 0 & 0 & 0 \\ 0 & 0.05 & 0 \\ 0 & 0 & 0 \end{bmatrix}. \quad (16)$$

$$\mathbf{A}_8 = \begin{bmatrix} 0 & 0 & 0 \\ 0.20 & 0.60 & 0.20 \\ 0 & 0 & 0 \end{bmatrix}, \quad \mathbf{B}_8 = \begin{bmatrix} 0 & 0 & 0 \\ 0 & 0.10 & 0 \\ 0 & 0 & 0 \end{bmatrix}. \quad (17)$$

For the $\mathbf{A}_7 - \mathbf{B}_7$ templates, cells along the diagonal with slope $m = +1$ become synchronized quite rapidly if the input image has a diagonal line with slope $m = +1$ (see Fig. 12). As illustrated by Figs. 13(b)–(i), horizontal neighboring cells become synchronized very rapidly (for the $\mathbf{A}_8 - \mathbf{B}_8$ templates) for the input image of Fig. 13(a) that is composed of three horizontal lines. An observation not included in the figures is that the synchronization is also achieved among cells along any line of the input image. In Fig. 13(j) and (k), it can be seen that no synchronization is obtained between cells belonging to different lines.

## IV. Conclusion

The results obtained by computer simulations on the 2-D array of $f(x) - \dot{x}$ coupled Chua's circuits give insight into the dynamics of the array. Our empirical analysis of mode and phase coherency and bifurcations as related to the connection weights and inputs can be used for further research on high-dimensional chaos and signal processing by chaotic arrays. It can also provide a basis for theoretical studies on the complex dynamics of 2-D arrays of Chua's circuits.

## Acknowledgment

The authors would like to thank L. O. Chua for his valuable comments.

## References

[1] C. Güzeliş, "Chaotic cellular neural networks made of Chua's circuits," in *Chua's Circuit: A Paradigm for Chaos*, R. N. Madan, Ed., *World Scientific Series on Nonlinear Science*, series B, vol. 1. Singapore: World Scientific, 1993, pp. 952–961,.

[2] V. N. Belykh, N. N. Verichev, Lj. Kocarev, and L. O. Chua, "On chaotic synchronization in a linear array of Chua's circuits," in *Chua's Circuit: A Paradigm for Chaos*, R. N. Madan, Ed., *World Scientific Series on Nonlinear Science*, series B, vol. 1. Singapore: World Scientific, 1993, pp. 325–335.

[3] A. M. Dabrowski, W. R. Dabrowski, and M. J. Ogorzalek, "Dynamic phenomena in chain interconnections of Chua's circuits," *IEEE Trans. Circuits Syst.*, vol. 40, pp. 868–871, Nov. 1993.

[4] M. J. Ogorzalek, A. M. Dabrowski, and W. R. Dabrowski, "Hyperchaos, clustering and cooperative phenomena in CNN arrays composed of chaotic circuits," in *Proc. Third IEEE Int. Workshop on Cellular Neural Networks and Their Applicat.*, CNNA '94, Rome, 1994, pp. 315–320.

[5] C. Güzeliş and L. O. Chua, "Stability analysis of generalized cellular neural networks," *Int. J. Circuit Theory Applicat.*, pp. 1–33, 1993.

[6] K. Kaneko, "Clustering, coding, switching, hierarchial ordering and control in a network of chaotic elements," *Physica D*, vol. 41, pp. 137–172, 1990.

[7] W. J. Freeman, "Tutorial on neurobiology: from single neurons to brain chaos," *Int. J. Bifurc. and Chaos*, vol. 2, no. 3, pp. 451–482, 1992.

[8] B. Baird, M. W. Hirsch, and F. Eeckman, "A neural network associative memory for handwritten character recognition using multiple Chua attractors," *IEEE Trans. Circuits Syst. II*, vol. 40, pp. 667–674, 1993.

[9] L. O. Chua, "The genesis of Chua's circuit," *Arch. Elekt. Ubertragung.*, vol. 46, pp. 250–257, 1992.

[10] K. Murali and M. Lakshmanan, "Effects of sinusoidal excitation on the Chua's circuit," *IEEE Trans. Circuits Syst.*, vol. 39, pp. 267–270, 1992.

[11] J. M. Cruz and L. O. Chua, "A CMOS IC nonlinear resistor for Chua's circuit," *IEEE Trans. Circuits Syst.*, vol. 39, pp. 985–995, 1992.

[12] M. P. Kennedy, "Robust op amp implementation of Chua's circuit," *Frequenz*, vol. 46, pp. 66–80, 1992.

[13] L. O. Chua and L. Yang, "Cellular neural networks: Theory and applications," *IEEE Trans. Circuits Syst.*, vol. 35, pp. 1257–1272, 1988.

[14] V. Perez-Munuzuri, V. Perez-Villar, and L. O. Chua, "Traveling wave front and its failure in a one dimensional array of Chua's circuits," in *Chua's Circuit: A Paradigm for Chaos*, R. N. Madan, Ed., *World Scientific Series on Nonlinear Science*, series B, vol. 1. Singapore: World Scientific, 1993, pp. 336–350.

[15] ——, "Autowaves for image processing on a two dimensional CNN array of excitable nonlinear Chua's circuits: Flat and wrinkled labyrinths," *IEEE Trans. Circuits Syst.*, vol. 40, pp. 174–181, Mar. 1993.

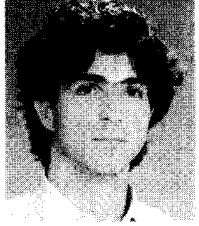

**Fatih Kavaslar** received the B.S. and M.S. degrees in electrical engineering from İstanbul Technical University, Turkey in 1991 and 1995, respectively. He is currently a Ph.D. student in electrical engineering at İstanbul Technical University.

In 1992, he joined Siemens Company, İstanbul, as a member of the Power Electronics Division. He won the 1989 Turkish championship in fin sailing. His research interests are in digital signal processing, neural networks, and computer vision.

**Cüneyt Güzeliş** received the B.S., M.S., and Ph.D. degrees in electrical engineering from İstanbul Technical University, Turkey in 1981, 1984, and 1988, respectively.

He worked at İstanbul Technical University as a Teaching Assistant between 1982 and 1989. From April 1989 to April 1991, he was a visiting Researcher and Lecturer with the Department of Electrical Engineering and Computer Sciences, University of California at Berkeley. He joined İstanbul Technical University in 1991 where he now is an Associate Professor in the Faculty of Electrical-Electronics Engineering. His research interests are in nonlinear circuits and systems, neural networks, and signal processing.